AD-A114 311 RICE UNIV HOUSTON TX F/G 4/1
MODELING OF HIGH-LATITUDE CURRENTS IN A SUBSTORM,(U)
DEC 81 J L KARTY, C - CHEN, R A WOLF, M HAREL F19628-80-C-0009
UNCLASSIFIED SCIENTIFIC-1 AFGL-TR-81-0363 NL

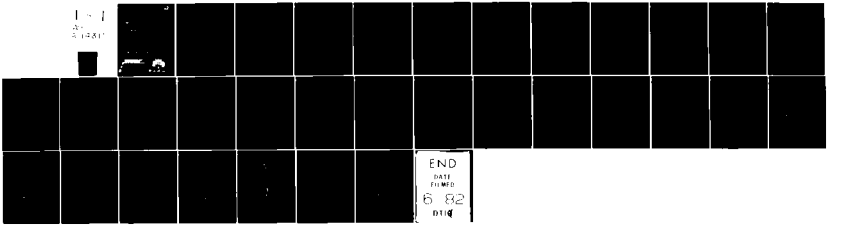

END
DATE FILMED
6 82
DTIC

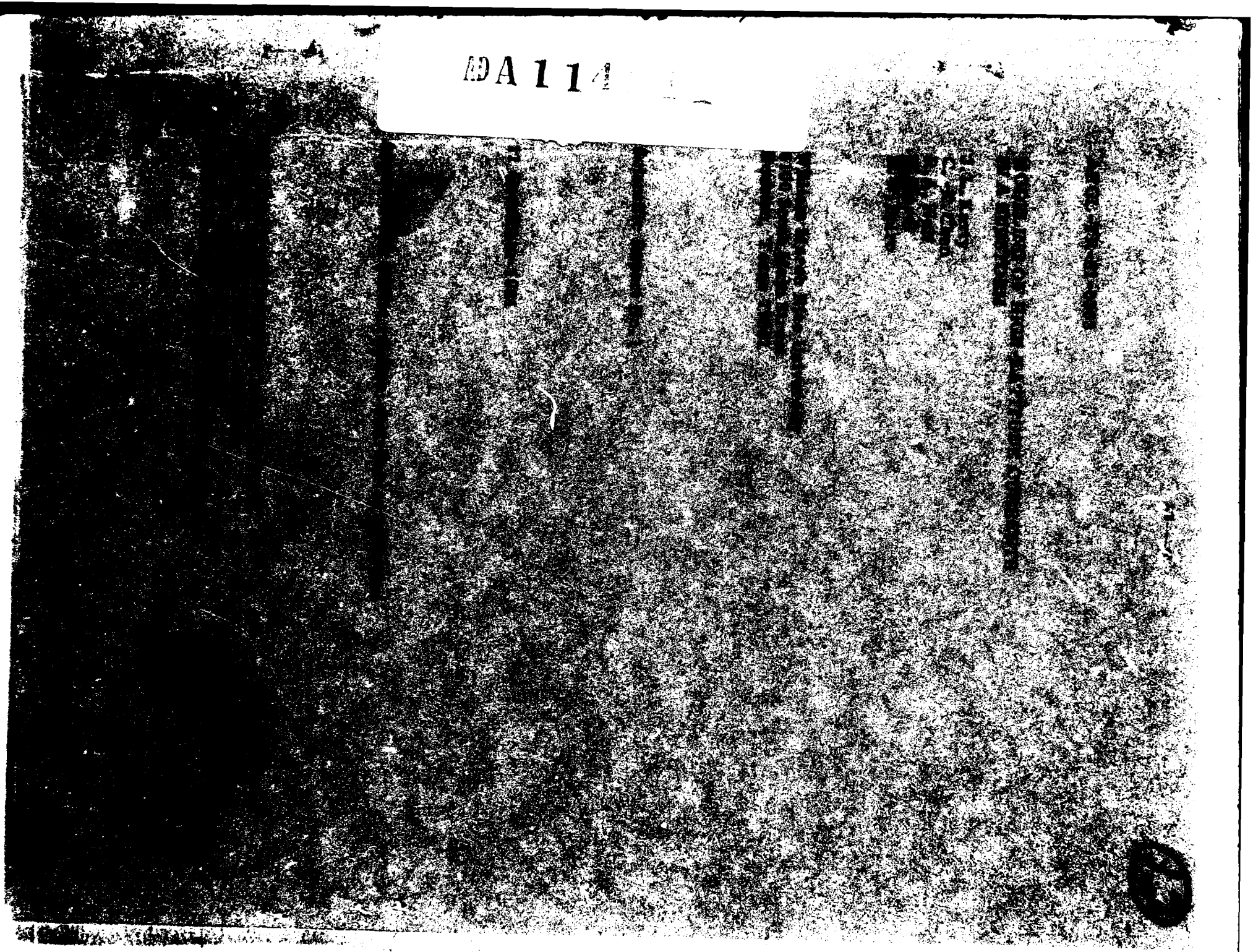
AD A 11

Unclassified
SECURITY CLASSIFICATION OF THIS PAGE (When Data Entered)

REPORT DOCUMENTATION PAGE

READ INSTRUCTIONS BEFORE COMPLETING FORM

1. REPORT NUMBER: AFGL-TR-81-0363
2. GOVT ACCESSION NO.: AD-A114 311
3. RECIPIENT'S CATALOG NUMBER:
4. TITLE (and Subtitle): MODELING OF HIGH-LATITUDE CURRENTS IN A SUBSTORM
5. TYPE OF REPORT & PERIOD COVERED: Scientific report no. 1
6. PERFORMING ORG. REPORT NUMBER:
7. AUTHOR(s): J. L. Karty, C.-K. Chen, R. A. Wolf, M. Harel, and R. W. Spiro
8. CONTRACT OR GRANT NUMBER(s): F19628-80-C-0009
9. PERFORMING ORGANIZATION NAME AND ADDRESS: William Marsh Rice University, 6100 South Main St., Houston, TX 77001
10. PROGRAM ELEMENT, PROJECT, TASK AREA & WORK UNIT NUMBERS: 61102 F, 2311 G2CC
11. CONTROLLING OFFICE NAME AND ADDRESS: Air Force Geophysics Laboratory, Hanscom AFB, Massachusetts 01731, Contract Monitor William J. Burke/PHG
12. REPORT DATE: 11 December 1981
13. NUMBER OF PAGES: 31
14. MONITORING AGENCY NAME & ADDRESS (if different from Controlling Office):
15. SECURITY CLASS. (of this report): Unclassified
15a. DECLASSIFICATION DOWNGRADING SCHEDULE:
16. DISTRIBUTION STATEMENT (of this Report): Approved for public release; distribution unlimited.
17. DISTRIBUTION STATEMENT (of the abstract entered in Block 20, if different from Report):
18. SUPPLEMENTARY NOTES:
19. KEY WORDS (Continue on reverse side if necessary and identify by block number): Magnetosphere, Ionosphere, Substorm
20. ABSTRACT (Continue on reverse side if necessary and identify by block number):

(Please see other side)

DD FORM 1 JAN 73 1473 EDITION OF 1 NOV 65 IS OBSOLETE

Unclassified
SECURITY CLASSIFICATION OF THIS PAGE (When Data Entered)

ABSTRACT

A quantitative model is developed for computing currents and electric fields in the area covered by the poleward set of field-aligned currents (region-1 Birkeland currents). The high-latitude band considered carries most of the westward electrojet and lies just poleward of the region treated in the Rice University computer simulation (which covers the inner magnetosphere and corresponding ionosphere); the present high-latitude-current model supplements the inner-magnetosphere simulations to make them nearly global. Birkeland current and aurorally enhanced conductivity are assumed to be uniformly distributed across the band. The area poleward of the band is taken to be an insulator, while boundary conditions at the low-latitude edge of the band are derived from the results of the lower-latitude computer simulations of the substorm event that occurred on September 19, 1976. The time-dependent conductivity model used is based on electron fluxes and mean energies measured from the Air Force S3-2 satellite. Ionospheric electric fields and currents are calculated; ionospheric neutral winds are neglected.

Model predictions of the locations of the electric-field reversal agree well with typical OGO-6 satellite observations. The model also agrees with S3-2 data from September 19, 1976 on an important feature, namely, the electric field reversal usually occurs poleward of the bulk of region-1 current. Joule heating of the upper atmosphere, as inferred from calculation of currents and electric fields in the high-latitude region considered here, was found to be about 2×10^{11} watts during the substorm period, somewhat less than the value estimated for the lower-latitude region (region-2 and below). Model values for the strength of the electrojet and the amount of Joule heating agree to within ~ 20% with results based on a simple Cowling conductivity band (with no latitudinal current flowing into the band).

10 to the 11th power

I. INTRODUCTION

Work at Rice University over the past few years has produced a method of computer simulating convection in the inner magnetosphere ($L \lesssim 10$). The Rice Convection Model self-consistently includes ionospheric, Birkeland and ring currents [Jaggi and Wolf, 1973; Harel and Wolf, 1976; Harel et al., 1981a]. Recently, two geophysical events--the substorm-type event of September 19, 1976 and the magnetic storm of July 29, 1977--have been computer simulated, and theoretical predictions have been compared with a variety of observational data [Harel et al., 1981b; Spiro et al., 1981; Wolf et al., 1981]. The region of applicability of the Rice Convection Model has been restricted to the inner magnetosphere. Uncertainties about the detailed physics governing solar-wind/magnetosphere coupling and magnetotail dynamics have prevented us from including the magnetopause boundary layer, the tail lobe and the outer plasma sheet in the self-consistent modeling scheme. In other words, we exclude from the self-consistent simulations [Harel et al., 1981a] the part of the magnetosphere that serves as the generator for magnetospheric convection [Stern, 1977]. Part of the auroral ionosphere has also been excluded, namely, the polar cap and the part of the ionosphere that corresponds to the region-1 Birkeland currents, which connect the ionosphere to the generator of the magnetospheric-convection system. [See, e.g., Schield et al., 1969; Wolf, 1974; or Stern, 1977.] The effect of the generating currents on inner-magnetospheric convection has been represented by a boundary condition.

Exclusion of the high-latitude part of the auroral zone from the modeling region has proved awkward in several respects. Most of the westward electrojet flows in the high-latitude part of the auroral zone. Neglecting the high-latitude ionospheric currents consequently precludes any serious comparisons

between theoretical and observed ground-magnetometer data. It also precludes accurate calculation of global Joule heating.

The present model represents an extension of the Rice Convection Model to the highest-latitude part of the auroral ionosphere. Although we cannot yet reliably computer simulate the physics of the far-magnetosphere ends of these field lines, we can model their ionospheric ends, using observational information and simple assumptions about the distribution of current coming down from the magnetosphere.

Many other theoretical models [Yasuhara et al., 1975; Yasuhara and Akasofu, 1977; Gizler et al., 1979; Nisbet et al., 1978; Nopper and Carovillano, 1978, 1979; Kamide and Matsushita, 1979a, 1979b] have treated the relationship between horizontal ionospheric currents and field-aligned currents. However, in these approaches, "typical" or "average" conditions of magnetic activity were considered, and only a general comparison with data was possible. Most studies use an average Birkeland current distribution as input, with a relatively simple conductivity model. Akasofu et al. [1980] have used data from the Alaska meridian magnetometer chain to infer Birkeland and horizontal ionospheric currents. On the other hand, the Rice Convection Model [Harel et al., 1981a, 1981b] does detailed simulations of individual events for more precise comparison with various types of data.

The model described in this paper complements the Rice Convection Model. The model uses polar cap potential drop and fairly realistic conductivity as input to compute Birkeland currents, electric fields, and horizontal ionospheric currents.

The modeled region is a band ~ 3° wide, centered at about 70-73° in geomagnetic latitude. More precisely, the low-latitude boundary of the band discussed in this paper is the low-latitude edge of region-1 Birkeland current.

The poleward boundary of the band is defined by the poleward extent of the aurorally enhanced conductivity, as inferred from satellite observations. The exact locations of the boundaries are variable.

The following section presents a detailed explanation of the theory. In the third section, this theory is applied to a specific substorm-type event that occurred on September 19, 1976. East-west "electrojet" currents and Joule heating rates are calculated for our modeling region for this event. Birkeland current strengths and electric field reversal locations are compared with average or typical satellite data. The impact of these high-latitude currents on ground magnetic variations is discussed in a separate paper [Chen et al., 1981].

II. THEORY

Current conservation implies that field-aligned current is balanced by the divergence of horizontal ionospheric current. Thus, current conservation can be expressed as

$$\nabla \cdot \underset{\sim}{j} = -j_{\parallel} \tag{1}$$

where $\underset{\sim}{j}$ is equal to the (height-integrated) horizontal current density flowing in the ionosphere, and $j_{\parallel}$ is equal to the density of upward field-aligned current. (Here, the divergence operator is two-dimensional.)

Ohm's law for ionospheric currents

$$\underset{\sim}{j} = \underset{\approx}{\Sigma} \cdot \underset{\sim}{E} \tag{2}$$

is used (neglecting neutral winds), where $\underset{\sim}{E}$ is the electric field in the frame of reference that rotates with the solid earth, and $\underset{\approx}{\Sigma}$ is the tensor representing height-integrated conductivity [Wolf, 1970; Jaggi and Wolf, 1973; Rishbeth and Garriott, 1969, p. 138]:

$$\underset{\approx}{\Sigma} = \begin{pmatrix} \Sigma_{\xi\xi} & \Sigma_{\xi\psi} \\ \Sigma_{\psi\xi} & \Sigma_{\psi\psi} \end{pmatrix}. \tag{3}$$

Here, $\Sigma_{\xi\xi} = \Sigma_P/\sin^2 I$, $\Sigma_{\xi\psi} = -\Sigma_{\psi\xi} = \Sigma_H/\sin I$, and $\Sigma_{\psi\psi} = \Sigma_P$, where Σ_P and Σ_H are height-integrated Pedersen and Hall conductivities, respectively, and I is the magnetic dip angle. Combining (1), (2), and $\underset{\sim}{E} = -\nabla V$, where V is the electrostatic potential (assuming that any induction fields are negligible), we get:

$$\nabla \cdot (\underset{\approx}{\Sigma} \cdot \nabla V) = j_{\parallel}. \tag{4}$$

Within the band, conductivity depends on local time, but is independent of latitude. A thin band is assumed (i.e., the band width is small compared to the distance to the pole). For a thin band, the azimuthal component of electric field is approximately independent of distance across the band, since $\nabla \times \underset{\sim}{E} = 0$ implies (by Stokes' law) that $\int \underset{\sim}{E} \cdot d\underset{\sim}{\ell} = 0$. We assume Birkeland current to be independent of latitude within the modeling region. With this assumption, and within the thin band approximation, current conservation implies that horizontal ionospheric currents and the poleward component of the electric field vary almost linearly with latitude.

Figure 1 presents a definition of coordinates used in the model. As an approximation, the polar cap is taken to be flat. A two-dimensional polar coordinate system is used. (The center of the coordinate system is offset

from the geomagnetic pole by two degrees toward midnight). Boundary conditions are:

$$V = V(\psi) \text{ at } \xi = a, \tag{5}$$

$$j_\xi = g(\psi) \text{ at } \xi = a, \text{ and} \tag{6}$$

$$j_\xi = 0 \text{ at } \xi = b(\psi). \tag{7}$$

(Equation (7) follows from the approximation that the polar cap is an insulator.) We write the azimuthal electric field in the form:

$$E_\psi(\xi,\psi) = -\frac{1}{\xi}\frac{\partial V(\xi,\psi)}{\partial\psi} \simeq -\frac{1}{\xi}\frac{dV(\psi)}{d\psi}. \tag{8}$$

(In the thin-band approximation, we neglect the ξ-dependence of $\partial V(\xi,\psi)/\partial\psi$.) The latitudinal components of electric field at b and a are evaluated using equation 8, the boundary conditions given by equations 6 and 7, and Ohm's law for ionospheric currents (equation 2). We obtain:

$$E_\xi(b,\psi) = \frac{\Sigma_{\xi\psi}(\psi)}{\Sigma_{\xi\xi}(\psi)}\frac{1}{b}\frac{dV(\psi)}{d\psi}, \text{ and} \tag{9}$$

$$E_\xi(a,\psi) = \frac{[g(\psi) + \Sigma_{\xi\psi}(\psi)\frac{1}{a}\frac{dV(\psi)}{d\psi}]}{\Sigma_{\xi\xi}(\psi)}. \tag{10}$$

We assume that $E_\xi(\xi,\psi)$ varies linearly between b and a. Using the linear dependence of E_ξ on ξ, and integrating leads immediately to an expression for $V(\xi,\psi)$. Evaluation of this expression at $\xi = a$ confirms self-consistency of the potential used with assumed boundary conditions.

From a knowledge of $E_\xi(\xi,\psi)$ and $E_\psi(\xi,\psi)$, total east-west current (i.e., the "electrojet"), and Joule heating can be calculated. Total eastward current is given by:

$$J_\psi = \int_b^a j_\psi d\xi = \Sigma_{\psi\psi}(\psi)\,\frac{dV(\psi)}{d\psi}\,\ell n\left(\frac{b}{a}\right) - \Sigma_{\xi\psi}(\psi)\left(\frac{E_\xi(a,\psi) + E_\xi(b,\psi)}{2}\right)(a - b). \quad (11)$$

Joule heating (per unit ψ) is given by:

$$JH = \int_b^a \underset{\sim}{j} \cdot \underset{\sim}{E}\xi\, d\xi = \int_b^a \{\Sigma_{\xi\xi}(\psi)[E_\xi(\xi,\psi)]^2$$

$$+ \Sigma_{\psi\psi}(\psi)[E_\psi(\xi,\psi)]^2\}\xi\, d\xi. \quad (12)$$

This becomes:

$$JH = \Sigma_{\psi\psi}(\psi)\left(\frac{dV(\psi)}{d\psi}\right)^2 \ell n\,(a/b) + \Sigma_{\xi\xi}(\psi)\left(\frac{a - b}{6}\right)\{[E_\xi(b,\psi)]^2\left(\frac{a + 3b}{2}\right)$$

$$+ E_\xi(b,\psi)\,E_\xi(a,\psi)(a + b) + [E_\xi(a,\psi)]^2\left(\frac{b + 3a}{2}\right)\}. \quad (13)$$

With ionospheric current, Birkeland current is calculated from current conservation. Multiplying (1) by $\xi d\xi$ and integrating from $\xi = b$ to $\xi = a$ gives

$$-\int_b^a j_\parallel \xi\, d\xi = \int_b^a \frac{\partial(\xi j_\xi)}{\partial\xi}\, d\xi + \int_b^a \frac{\partial j_\psi}{\partial\psi}\, d\xi.$$

This is equivalent to:

$$\frac{dJ_\parallel}{d\psi} = -\frac{dJ_\psi}{d\psi} - \frac{dJ_\xi}{d\psi}, \quad (14)$$

where $\frac{dJ_\parallel}{d\psi}$ and $\frac{dJ_\xi}{d\psi}$ are, respectively, the total Birkeland and equatorward currents leaving the band per unit ψ.

III. APPLICATION OF MODEL TO SEPTEMBER 19, 1976 SUBSTORM EVENT

Harel et al. [1981a, 1981b] have simulated the substorm event of September 19, 1976. Figure 3 of Harel et al. [1981a] shows the Fort Churchill H magnetogram and the estimated potential drop for the event. Onset of the event occurred at approximately 1000 UT. Figures 2a and 2b show the equatorward boundary conditions that were furnished by the original simulation and were used as input to the present high-latitude model. The figures correspond to 1100 UT, near the observed peak of substorm activity.

The conductivity model considers auroral enhancement and photoionization. (Our method of including the sunlight effect is described by Harel et al. [1981a, pg. 2234].) At the high latitudes considered in the present model, auroral enhancement is the dominant effect. We use equations (9) and (10) of Harel et al. [1981a] to infer auroral conductivity enhancements from electron fluxes and average energies measured by the S3-2 satellite [D. A. Hardy, private communication, 1977]. (See Wallis and Budzinski [1981] for a comparison of equations [9] and [10] with more precise calculations.) Integration of satellite data over a distance defined by electron flux enhancement, and then fitting the data to a trigonometric function of local time, provides the auroral enhancement conductivity model. Actual measurements were near dawn and dusk, so the that all other local times were obtained by extrapolation. The model allows auroral conductivity enhancement at midnight to be ~ 4 times greater than the conductivity enhancement at noon, for the high-latitude area treated here. To obtain the total conductivity, contributions from the auroral enhancement, photoionization, and base-level nightside values are summed according to equations (A.20) and (A.21) of Harel et al. [1981a]. Figure 2c depicts the local-time dependent conductivity for 1100 UT. The

width of the band also depends on electron-flux measurements. Integration of satellite data over a distance defined by the region of high electron flux, and then fitting the data to a trigonometric function of local time, provides the model for the width of the band. The poleward boundary is taken to be a function of local time, but the equatorward boundary remains constant in this approach.

The Birkeland current pattern predicted from this model is compared with the observational data of Iijima and Potemra [1979, private communication] in Figure 3. Included in this figure is a plot (from Figure 2b) of $-j_\xi(a)$ (which is equal to Birkeland current if one neglects east-west current for $\xi < a$). The present calculation improves upon this approximation by including effects of the high-latitude auroral electrojet (which is known to intensify during a substorm). It should be emphasized that plotted data were statistically averaged for $|AL| > 100\ \gamma$ by Iijima and Potemra. The model predicted Birkeland-current strengths tend to be larger than the observational average, probably because $|AL|$ was about $600\ \gamma$ at 1100 UT.

An analysis of the dependences of Birkeland current and the electrojet (within the modeled region) on boundary conditions provides important physical insights. In this model, Birkeland current is mainly "controlled" by the latitudinal current at the equatorward boundary. Additionally, in a simple Cowling model, with $j_\xi = 0$ everywhere within the thin band, we have

$$J_\psi = \left(\Sigma_p + \frac{\Sigma_H^2}{\Sigma_p}\right) E_\psi\ (a - b), \tag{15}$$

so that the electrojet is equal to the product of the Cowling conductivity, the azimuthal component of electric field and the band width. Figure 4 shows that values from the Cowling conductivity picture agree with the present model

to within ~ 20%. Apparently, the total east-west current is mainly "controlled" by east-west electric field, which was essentially a boundary condition.

As illustrated in Figure 4, the calculated westward electrojet in the region treated in this paper (from equation 11) extends from about 1900 LT past midnight to about 0900 LT, with a maximum strength of ~ 11×10^5 amp in post-midnight hours. (This is in reasonable agreement with observational data for substorm conditions.) Figure 5 shows total ionospheric current density for geomagnetic latitudes poleward of ~ 60°. Current vectors displayed include both results from the present model and the lower latitude Rice simulation. Most of the westward electrojet lies in the high-latitude area of region-1 current. The calculated eastward electrojet is comparable to (but slightly weaker than) the portion of the eastward electrojet in the lower-latitude region; the lower latitude electrojet extends to ~ 2300 LT.

Theoretical magnetograms were computed and compared with observational data for the substorm event of September 19, 1976. Magnetic perturbations observed on the ground result mostly from the current systems in the Earth's ionosphere and magnetosphere. The details of the method used to calculate theoretical magnetograms can be found in Chen et al. [1981]. The Birkeland current and east-west currents in region-1 are part of a larger current system. It should be emphasized that since the westward electrojet flows mainly in the poleward region and has large ground magnetic effects, the addition of the auroral band described in this paper greatly improves agreement between theoretical and observed magnetograms. The comparison of theoretical and observed magnetograms is presented and discussed by Chen et al. [1981].

In the present model, it also is possible to investigate the location of electric field reversals. Figure 6 presents a diagram of the thin band and

the predicted global electric field reversal pattern for geomagnetic latitudes poleward of ~ 50°. The global pattern predicted from the model is in very good agreement with the observed pattern shown in Figure 7. In both Figures 6 and 7, the reversal is at ~ 75° geomagnetic latitude near dusk and dawn, whereas near midnight (in the classical Harang discontinuity region), the reversal appears at ~ 63° geomagnetic latitude. Overall concurrence of Figure 6 with observations is especially encouraging.

Values for Joule heating derived from this model (from equation 13) are shown graphically in Figure 8a for UT = 1100. In the simple Cowling conductivity example discussed previously, Joule heating per area is given by the expression:

$$JH = \Sigma_P \left(E_\xi^2 + E_\psi^2\right), \tag{16}$$

which is equivalent to

$$JH = \left(\Sigma_P + \frac{\Sigma_H^2}{\Sigma_P}\right) E_\psi^2. \tag{17}$$

In this picture, Joule heating (per length) is equal to the product of the Cowling conductivity, the square of the azimuthal component of the electric field, and the band width. Figure 8a shows that values from the Cowling conductivity picture (with no latitudinal current flowing into the band) agree with the present model to within ~ 20%. Since the azimuthal component of electric field is proportional to the derivative of the equatorward boundary potential (equation 8), the above discussion implies that Joule heating in the high-latitude band is mainly "controlled" by the equatorward boundary potential. A detailed background discussion on Joule heating is provided in Harel

et al. [1981b], along with results of their study. This effort helps to make the previous investigation more global. Figure 8b shows Joule heating contributions from both the present high-latitude model (indicated by circles) and the lower latitude simulation for 1100 UT. The high- and low-latitude regions tend to complement each other, so that the total Joule heating is relataively uniform as a function of local time. Included in Figure 9 are graphs indicating Joule heating and ring current energy as functions of universal time. The top panel indicates that the integrated (total) Joule heating is about 3.2 times the change in ring current energy for the modeled substorm. (See Harel et al. [1981b].) The bottom panel shows that Joule heating poleward of the equatorward edge of region-1 currents comprises ~ 40% of the total Joule heating in our modeled event. Clearly, the region we treat here makes a significant contribution to global Joule heating.

The prime incentive for this study was to investigate the extent to which the higher latitude area (poleward of the main simulation region of the Rice Convection Model) affected ground magnetic variations and Joule heating of the upper atmosphere. Addition of this auroral band of high conductivity has significantly improved calculated magnetograms. Improved agreement between observed and calculated magnetograms is due to inclusion of the large, often dominant, ground magnetic effects of the westward electrojet flowing mainly in the higher latitude region treated in this paper. In addition, this investigation indicated that the amount of Joule heating of the upper atmosphere inferred from calculations of currents and electric fields in the higher latitude region is significant.

ACKNOWLEDGMENTS

We are grateful to Dr. David A. Hardy for supplying unpublished electron-flux data from the S3-2 satellite. This work has been supported in part by the U.S. Air Force Geophysics Laboratory under grant F19628-80-C-0009 and in part by the Atmospheric Sciences Section of the National Science Foundation under grant ATM79-20157.

REFERENCES

Akasofu, S.-I., J. Kisabeth, G. J. Romick, H. W. Kroehl, and Byung-Ho Ahn, Day-to-day and average magnetic variations along the IMS Alaska meridian chain of observatories and modeling of a three-dimensional current system, J. Geophys. Res., 85, 2065, 1980.

Chen, C.-K., R. A. Wolf, M. Harel, J. L. Karty, Theoretical Magnetograms Based on Quantitative Simulation of a Magnetospheric Substorm, submitted to J. Geophys. Res., 1981.

Gizler, V. A., V. S. Semenov, and D. A. Troshichev, Electric fields and currents in the ionosphere generated by field-aligned currents observed by Triad, Planet. Space Sci., 27, 223, 1979.

Harel, M., and R. A. Wolf, Convection, in Physics of Solar-Planetary Environments, Vol. II., edited by D. J. Williams, (AGU: Washington, D. C.), p. 617, 1976.

Harel, M., R. A. Wolf, P. H. Reiff, R. W. Spiro, W. J. Burke, F. J. Rich, and M. Smiddy, Quantitative simulation of a magnetospheric substorm, 1. Model logic and overview, J. Geophys. Res., 86, 2217, 1981a.

Harel, M., R. A. Wolf, R. W. Spiro, P. H. Reiff, C.-K. Chen, W. J. Burke, F. J. Rich, and M. Smiddy, Quantitative simulation of a magnetospheric substorm, 2. Comparison with observations, J. Geophys. Res., 86, 2242, 1981b.

Iijima, T., and T. A. Potemra, The amplitude distribution of field-aligned currents at northern high latitudes observed by Triad, J. Geophys. Res., 81, 2165, 1976.

Iijima, T., and T. A. Potemra, Field-aligned currents in the dayside cusp observed by Triad, J. Geophys. Res., 83, 5971, 1976.

Iijima, T., and T. A. Potemra, Large-scale characteristics of field-aligned currents associated with substorms, J. Geophys. Res., 78, 599, 1978.

Jaggi, R. K., and R. A. Wolf, Self-consistent calculation of the motion of a sheet of ions in the magnetosphere, J. Geophys. Res., 78, 2852, 1973.

Kamide, Y., and S. Matsushita, Simulation studies of ionospheric electric fields and currents in relation to field-aligned currents. 1. Quiet periods, J. Geophys. Res., 84, 4083, 1979a.

Kamide, Y., and S. Matsushita, Simulation studies of ionospheric electric fields and currents in relation to field-aligned currents. 2. Substorms, J. Geophys. Res., 4099, 1979b.

Karty, J. L., The interaction of horizontal ionospheric and region one Birkeland currents, M.S. Thesis, Rice University, Houston, Texas, 1980.

Maynard, N. C., Electric field measurements across the Harang discontinuity, J. Geophys. Res., 79, 4620, 1974.

Nisbet, J. S. , J. M. Miller, and L. A. Carpenter, Currents and electric fields in the ionosphere due to field-aligned aurora currents, J. Geophys. Res., 83, 2647, 1978.

Nopper, R. W., and R. L. Carovillano, Ionospheric electric fields driven by field-aligned currents, in Quantitative Modeling of the Magnetospheric Processes, Vol. 21, edited by W. P. Olson, (Geophys. Monogr. Ser. AGU: Washington D. C.), p. 557, 1979.

Nopper, R. W., and R. L. Carovillano, Polar equatorial coupling during magnetically active periods, Geophys. Res. Lett., 5, 699, 1978.

Rishbeth, H. and O. K. Garriott, Introduction to Ionospheric Physics, (Academic Press: New York), 1969.

Schield, M. A., J. Freeman and A. J. Dessler, A source for field-aligned currents at auroral latitudes, J. Geophys. Res., 74, 247, 1969.

Spiro, R. W., M. Harel, R. A. Wolf, and P. H. Reiff, Quantitative simulation of a magnetospheric substorm, 3. Plasmaspheric electric fields and evolution of the plasmapause, J. Geophys. Res., 86, 2261, 1981.

Stern, D. P., Large-scale electric fields in the earth's magnetosphere, Rev. Geophys. Space Phys., 15, 156, 1977.

Wallis, D. D., and E. E. Budzinski, Emperical models of height integrated conductivities, J. Geophys. Res., 86, 125, 1981.

Wolf, R. A., Effects of ionospheric conductivity on convective flow of plasma in the magnetosphere, J. Geophys. Res., 75, 4677, 1970.

Wolf, R. A., Calculations of magnetospheric electric fields, in Magnetospheric Physics, edited by B. M. McCormac, (D. Reidel: Dordrecht, Holland), p. 167, 1974.

Wolf, R. A., and M. Harel, Dynamics of the magnetospheric plasma, in Dynamics of the Magnetosphere, edited by S.-I. Akasofu, (D. Reidel: Dordrecht, Holland), p. 143, 1979.

Wolf, R. A., M. Harel, R. W. Spiro, G.-H. Voigt, and C.-K. Chen, Computer simulation of inner magnetospheric dynamics for the magnetic storm of July 29, 1977, submitted to J. Geophys. Res., 1981.

Yasuhara, F., Y. Kamide, and S.-I. Akasofu, Field-aligned and ionospheric currents, Planet. Space Sci., 23, 1355, 1975.

Yasuhara, F., and S.-I. Akasofu, Field-aligned currents and ionospheric electric fields, J. Geophys. Res., 82, 1273, 1977.

FIGURE CAPTIONS

Figure 1. Polar view, illustrating definitions of coordinates used in the model.

Figure 2. (a) Equatorward boundary potential (used as input to model) as a function of local time (UT = 1100).

(b) Co-latitudinal component of horizontal ionospheric current at the equatorward boundary (used as input to model) as a function of local time (UT = 1100).

(c) Conductivity (used as input to model) as a function of local time (UT = 1100). ["o" refers to $\Sigma_{\xi\xi}$, "x" refers to $\Sigma_{\psi\psi}$, " " refers to $\Sigma_{\xi\psi}$.]

Figure 3. Birkeland current as a function of local time. Calculations from this paper are denoted by "•" (UT = 1100). For the simpler picture, in which $j_{\parallel} = -j_{\xi}$ (a), the curve is denoted by "x". Data from Iijima and Potemra (1979, private communication) are indicated by "Δ".

Figure 4. Total east-west current in our modeling region as a function of local time. Calculations using boundary conditions from lower latitude modeling are denoted by "o". Calculations using V(a) = 0 are denoted by "x". Calculations using $j_{\xi}(a) = 0$ (Cowling conductivity picture) are denoted by "Δ" (UT = 1100).

Figure 5. Ionospheric total current density. The two highest latitude "circles" of arrows are at the poleward and equatorward boundaries of the present high-latitude model. Arrows at lower latitudes are from results of the lower latitude computer simulation (UT = 1050).

Figure 6. Diagram of places where polarity reversals of radial electric field occur for UT = 1100. The dotted region is the band modeled here. The cross represents the geomagnetic north pole. The small dot at the center is the 2° offset discussed in the text. "●" refers to a reversal being inside the band. "x" refers either to a predicted reversal being poleward of the region studied (which physically means that the reversal must occur on the poleward boundary, as shown), or to a predicted reversal being at the equatorward boundary. "Δ" refers to predicted reversal positions from lower latitude (to 50°) studies of Harel et al. (1981a,b).

Figure 7. Schematic representations of typical convective flow and electric field directions looking down on north magnetic pole. The boundaries are for moderately disturbed to disturbed conditions. From Fig. 1 of Maynard [1974].

Figure 8. (a) High-latitude Joule heating per unit ψ (both hemispheres) as a function of local time. (See equations 12 and 13.) "o" refers to calculations using boundary conditions from lower latitude modeling; "x" refers to calculations for $V(a) = 0$; "Δ" refers to calculations for $j_\xi(a) = 0$, i.e., the Cowling-conductivity picture (UT = 1100).

(b) Joule heating per unit ψ (both hemispheres) as a function of local time showing contributions from both the high and low latitude models. "o" designates calculations from the present high-latitude model. Results from the lower latitude computer simulation are indicated by a solid line, with no symbols or label attached. The topmost curve is the sum of calculations from both the high latitude model and lower latitude simulation (UT = 1100).

Figure 9. The top panel shows ring current energy and integrated (total) Joule heating as functions of universal time through the event. The bottom panel shows Joule heating (both hemispheres) as a function of universal time through the modeled event. Calculations from this paper, i.e., due to the region of the ionosphere poleward of the equatorward edge of the region-1 currents, are indicated by "x". Calculations from Harel et al. [1981b], covering the region of the ionosphere equatorward of the equatorward edge of region-1 currents, are indicated by a solid line, with no symbols or label attached. The topmost curve is the sum of the other two curves, i.e., total Joule heating calculated in both the present high-latitude-current model and the lower latitude computer simulation. Initial substorm onset was at 10 UT, and activity remained high through 12 UT.

Scientists and engineers involved in the project:

J. L. Karty

C.-K. Chen

R. A. Wolf

M. Harel

R. W. Spiro

D. A. Hardy

Previous contracts:

F19628-77-C-0005

F19628-78-C-0078

Previously produced publications supported by the contract:

"Is steady convection possible in the earth's magnetotail?", by G. M. Erickson and R. A. Wolf, Geophys. Res. Lett., 7, 897, 1980.

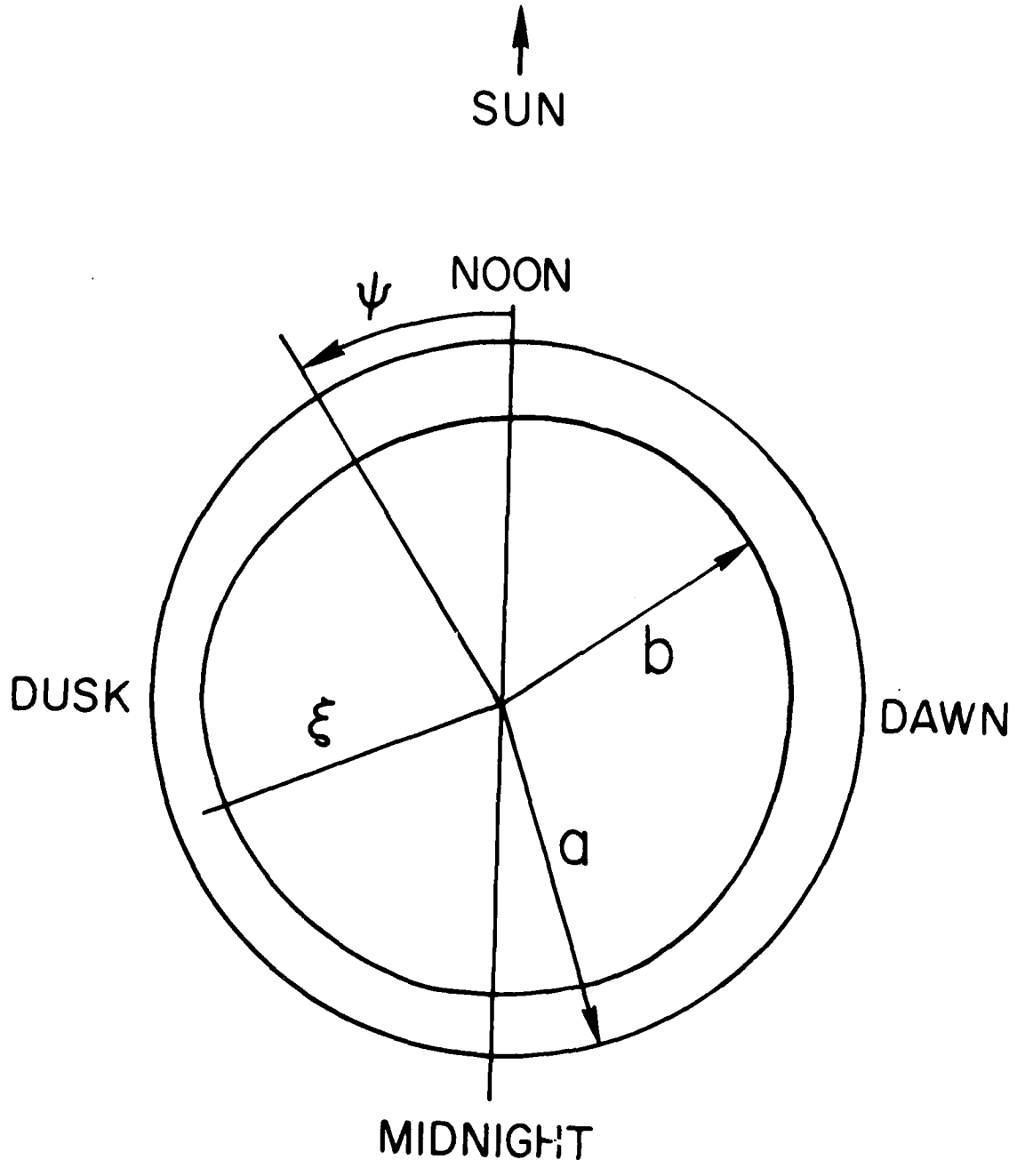

Figure 1

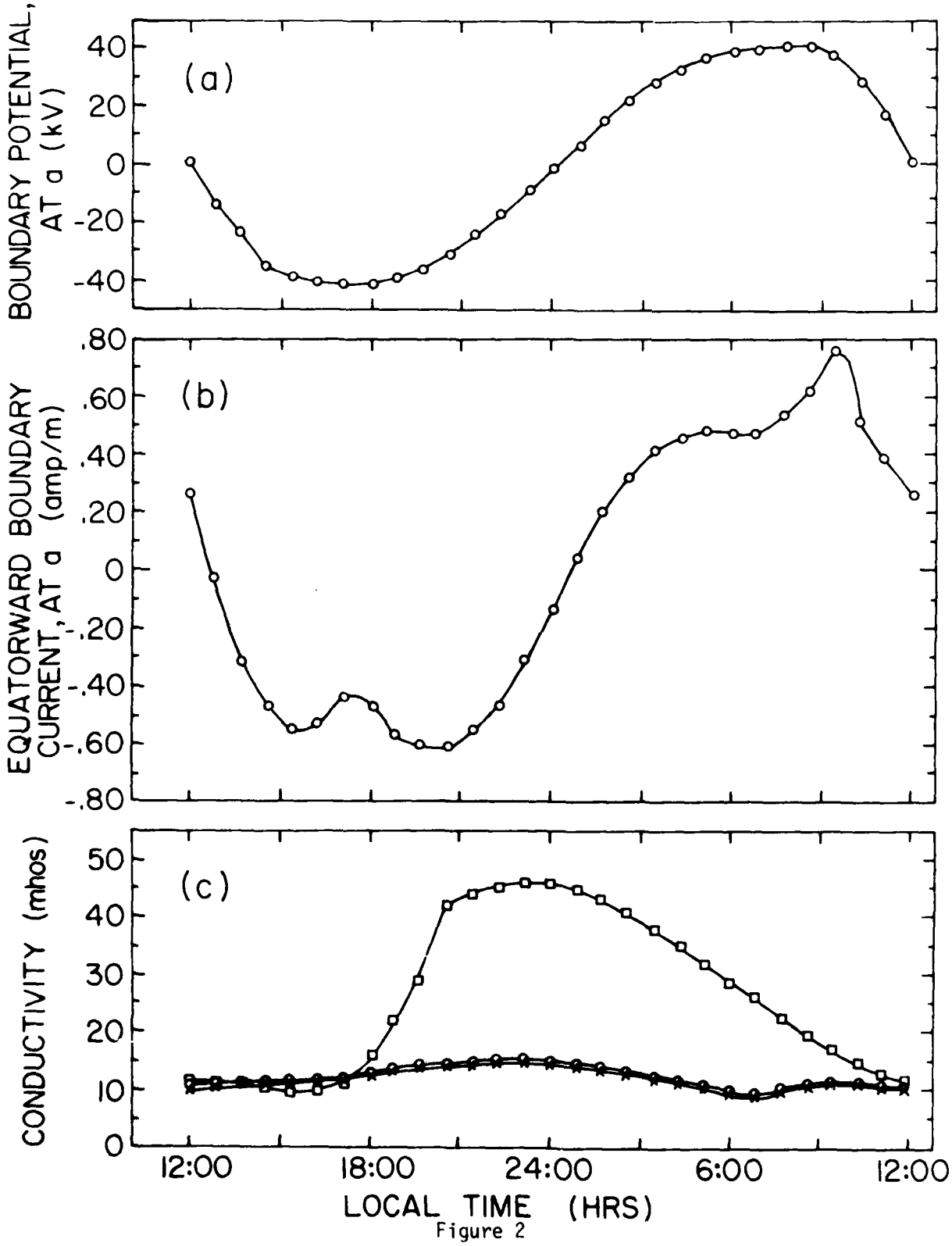
BOUNDARY POTENTIAL, AT a (kV)
40
20
0
-20
-40
(a)
EQUATORWARD BOUNDARY CURRENT, AT a (amp/m)
.80
.60
.40
.20
0
-.20
-.40
-.60
-.80
(b)
CONDUCTIVITY (mhos)
50
40
30
20
10
0
(c)
12:00
18:00
24:00
6:00
12:00
LOCAL TIME (HRS)

Figure 2

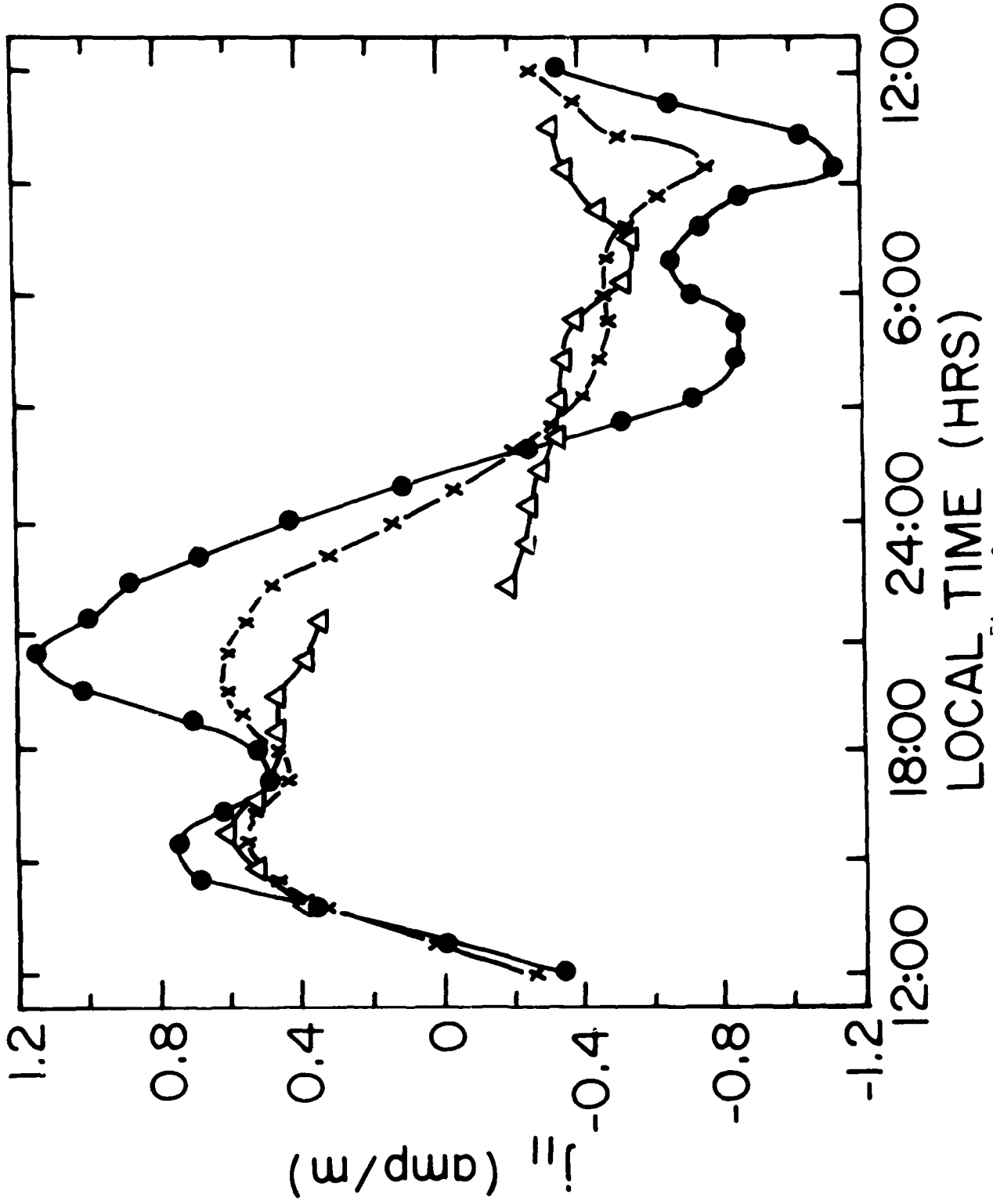
1.2
0.8
0.4
0
-0.4
-0.8
-1.2
$j_{\parallel}$ (amp/m)
12:00
18:00
24:00
6:00
12:00
LOCAL TIME (HRS)

Figure 3

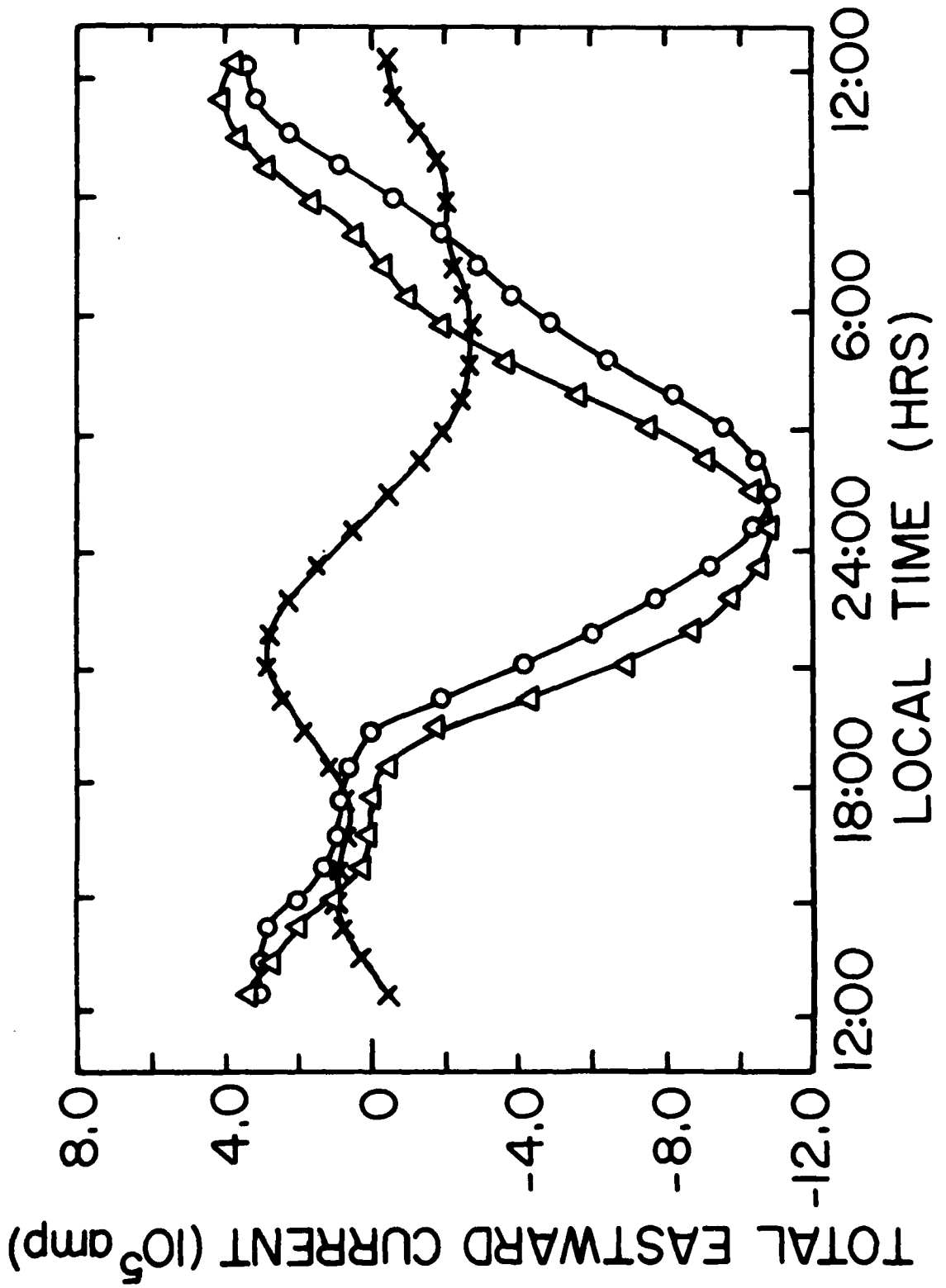
TOTAL EASTWARD CURRENT (10^5 amp)
8.0
4.0
0
-4.0
-8.0
-12.0
12:00
18:00
24:00
6:00
12:00
LOCAL TIME (HRS)

Figure 4

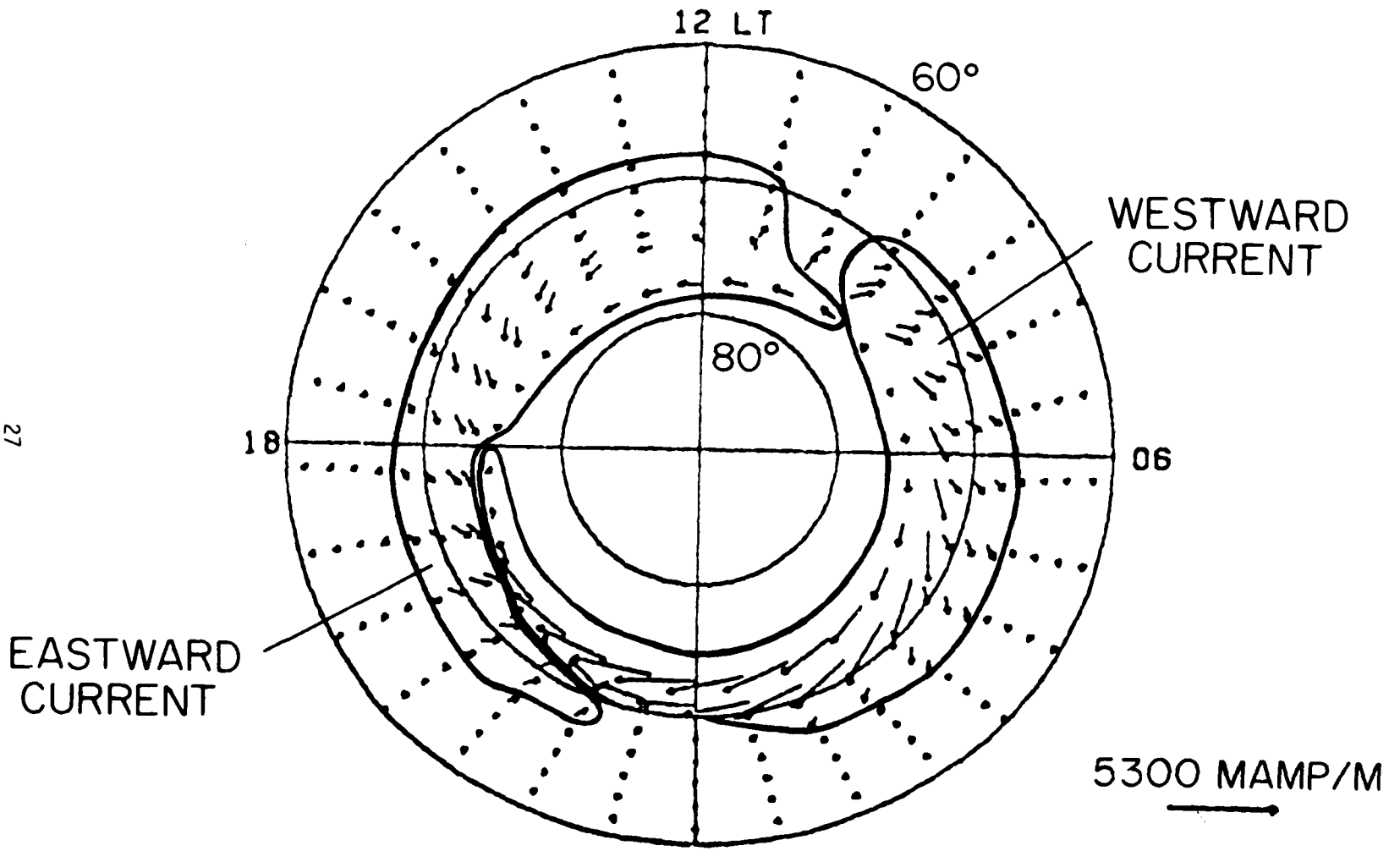
TIME = 10:50
12 LT
60°
80°
18
06
WESTWARD CURRENT
EASTWARD CURRENT
5300 MAMP/M

Figure 5

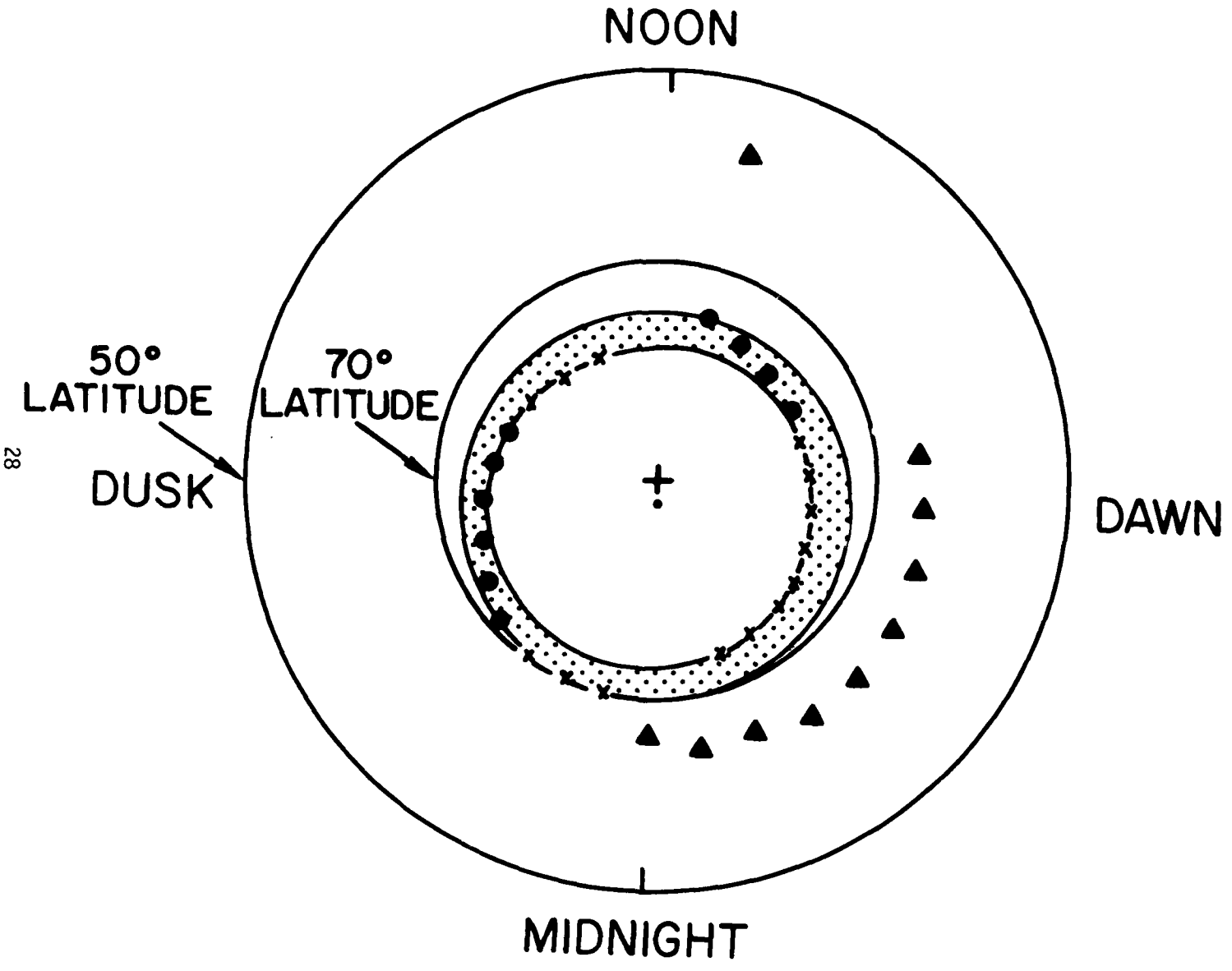

Figure 6

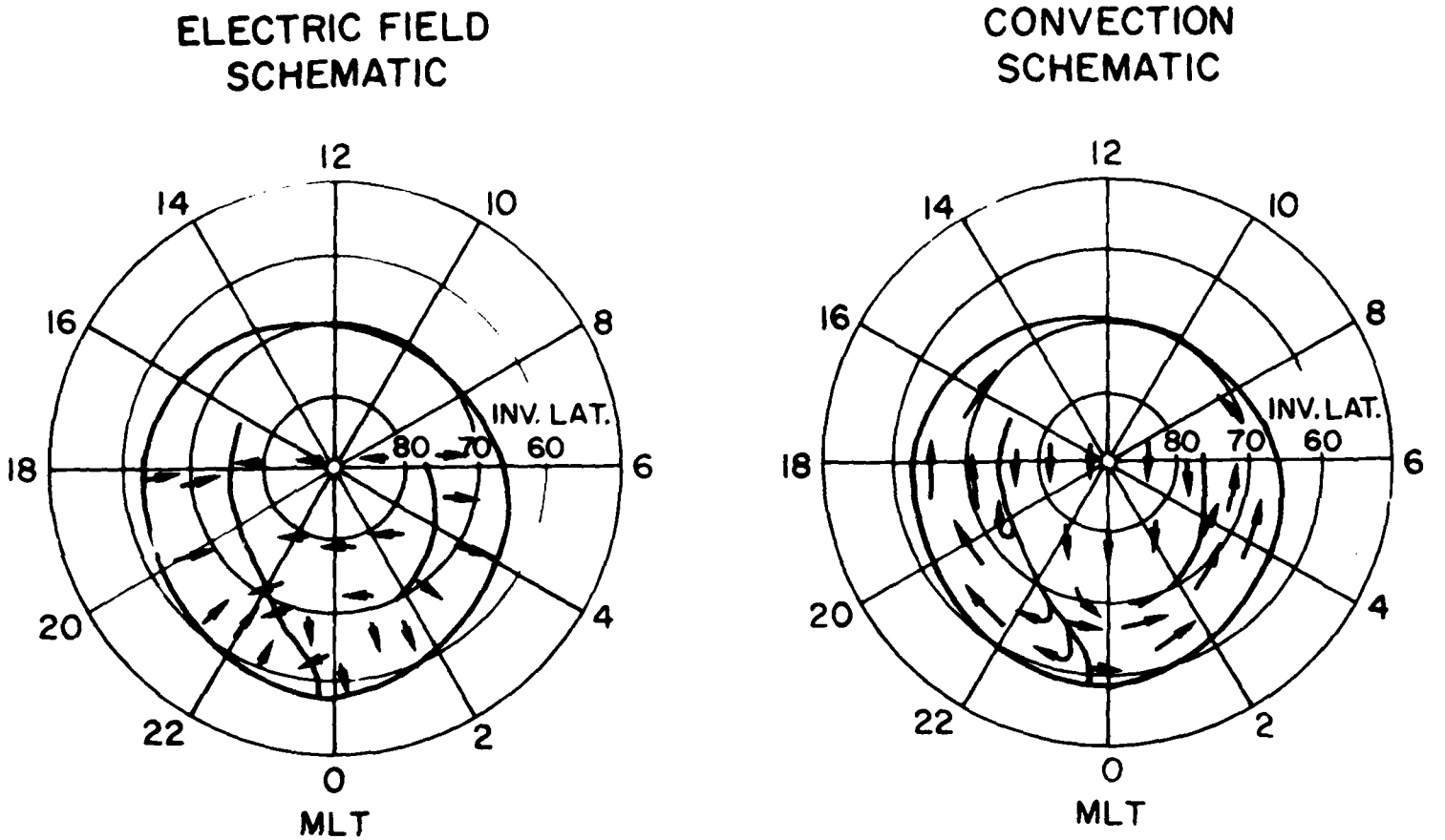
ELECTRIC FIELD
SCHEMATIC
12
14
10
16
8
18
6
20
4
22
2
0
MLT
INV. LAT.
80
70
60
CONVECTION
SCHEMATIC
12
14
10
16
8
18
6
20
4
22
2
0
MLT
INV. LAT.
80
70
60

Figure 7

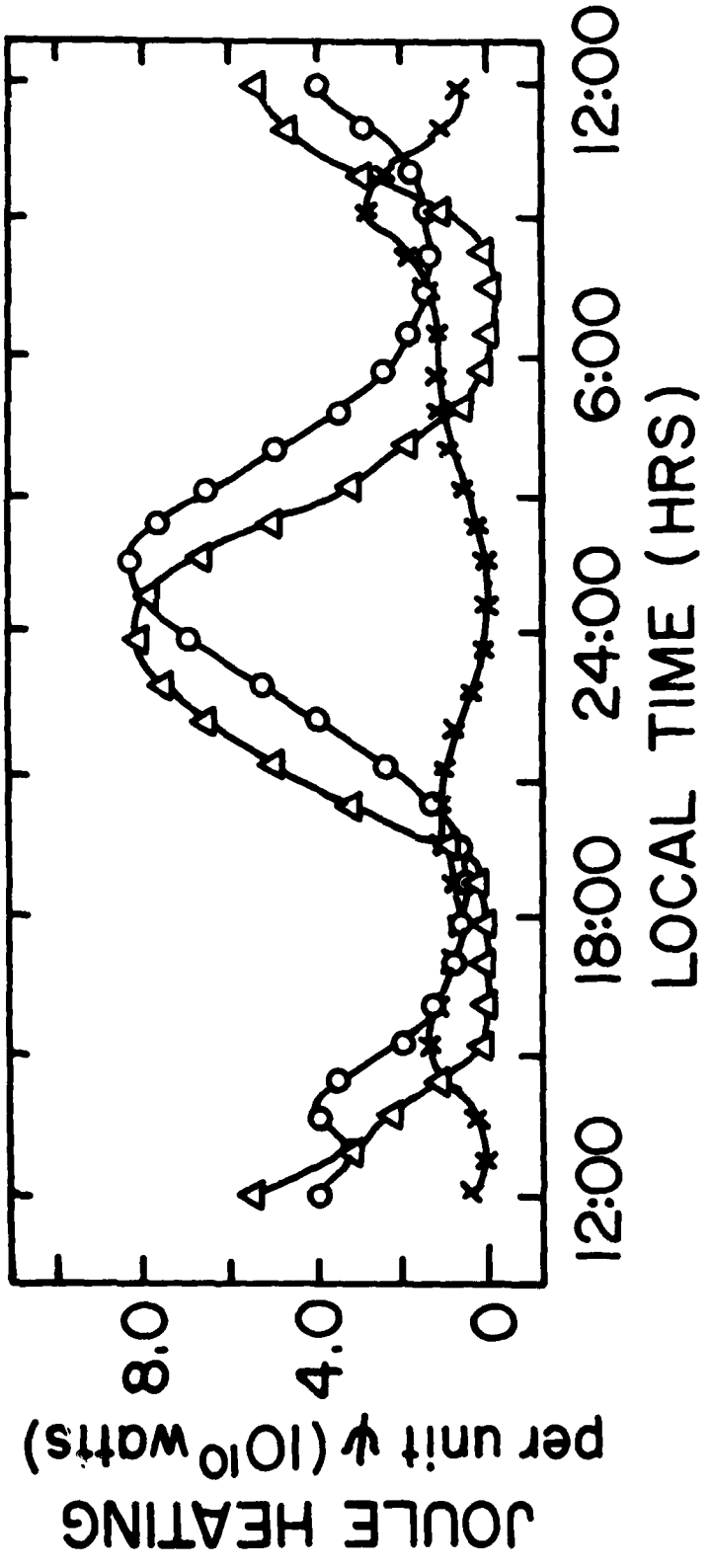
JOULE HEATING
per unit ψ (10^{10} watts)
8.0
4.0
0
12:00
18:00
24:00
6:00
12:00
LOCAL TIME (HRS)

Figure 8a

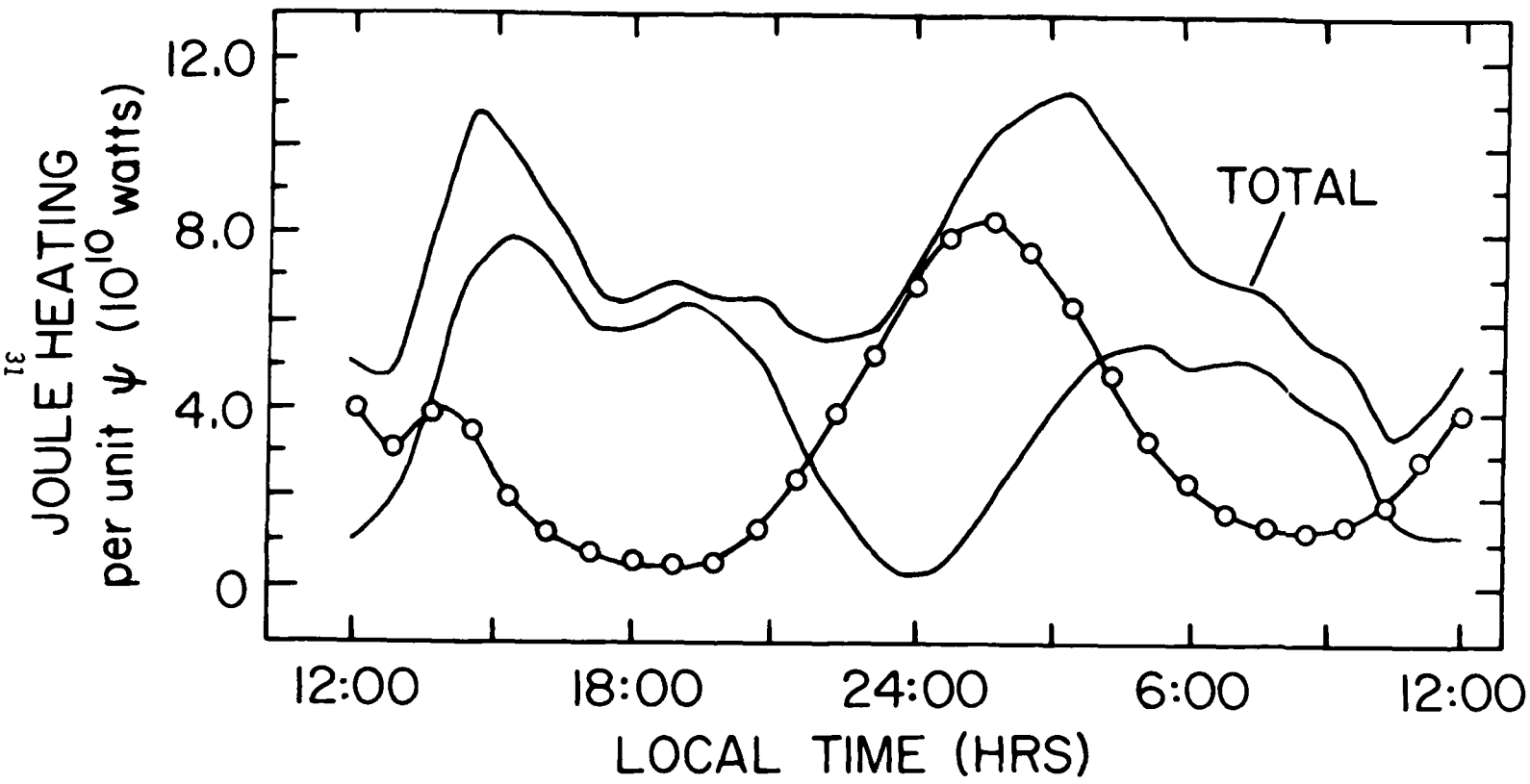
JOULE HEATING
per unit ψ (10^10 watts)
12.0
8.0
4.0
0
TOTAL
12:00
18:00
24:00
6:00
12:00
LOCAL TIME (HRS)

Figure 8b

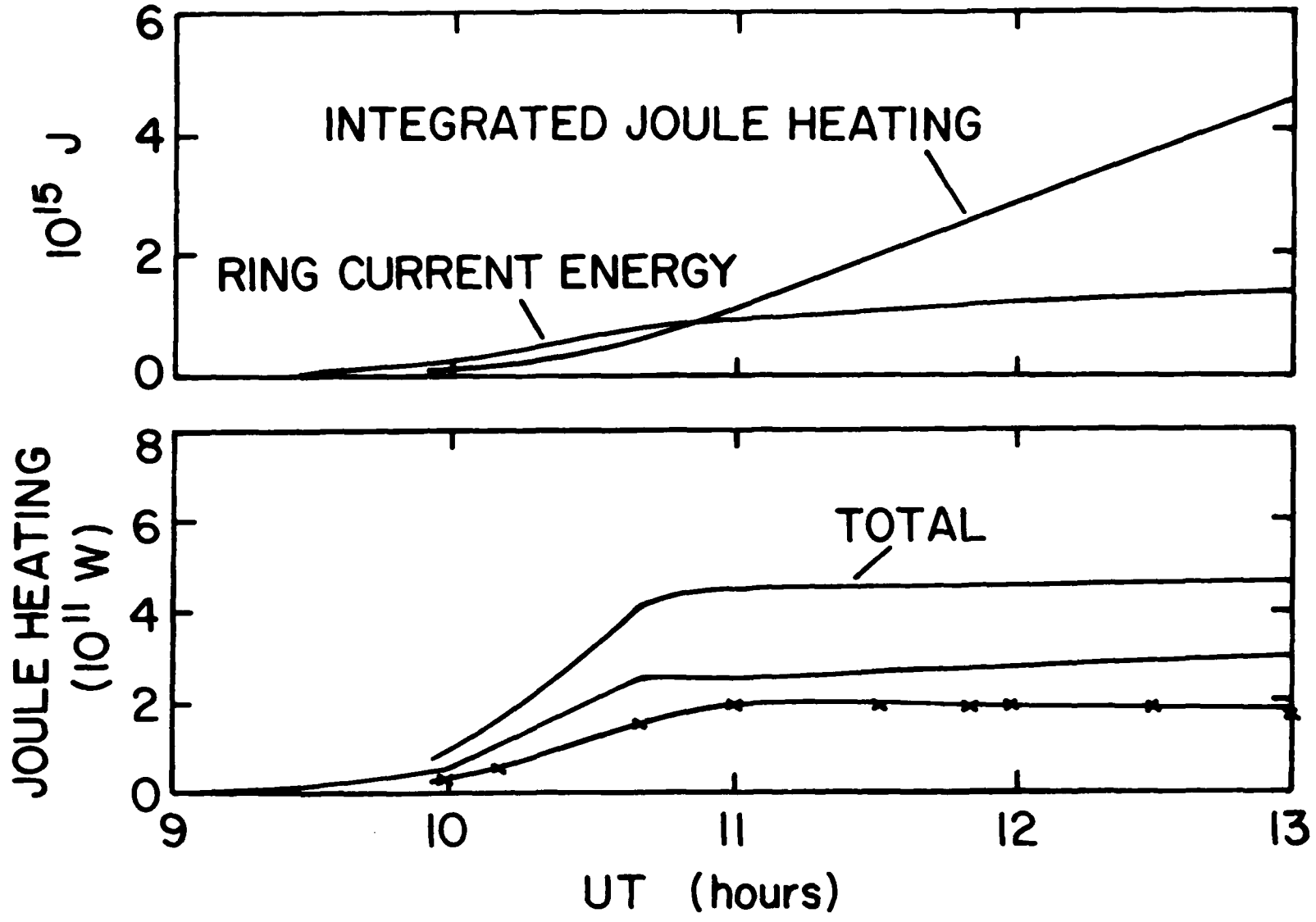
INTEGRATED JOULE HEATING
RING CURRENT ENERGY
10^{15} J
0
2
4
6
TOTAL
JOULE HEATING
(10^{11} W)
0
2
4
6
8
9
10
11
12
13
UT (hours)

Figure 9

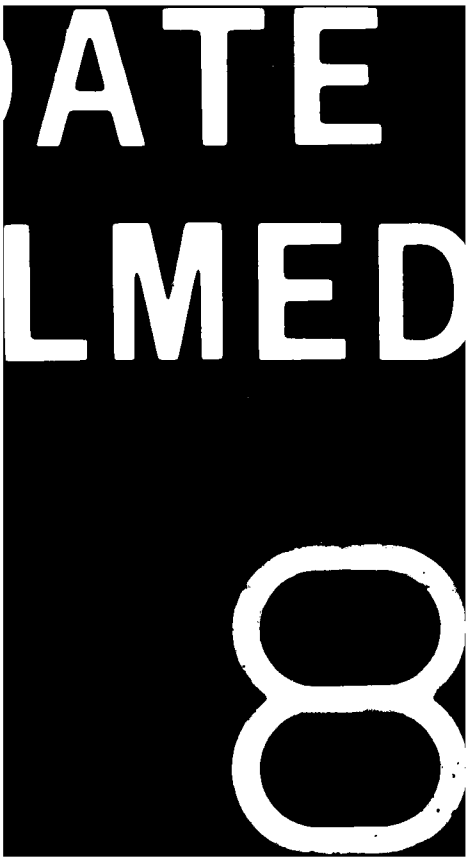
ATE
LMED
8